

Joint Cell Nuclei Detection and Segmentation in Microscopy Images Using 3D Convolutional Networks

Sundaresh Ram^{1,2}(✉), Vicky T. Nguyen³, Kirsten H. Limesand³, and Mert R. Sabuncu^{1,2}

¹ School of Electrical & Computer Engineering, Cornell University, Ithaca, NY, USA
sr2255@cornell.edu

² Nancy E. & Peter C. Meinig School of Biomedical Engineering, Cornell University, Ithaca, NY, USA

³ Department of Nutritional Sciences, University of Arizona, Tucson, AZ, USA

Abstract. We propose a 3D convolutional neural network to simultaneously segment and detect cell nuclei in confocal microscopy images. Mirroring the co-dependency of these tasks, our proposed model consists of two serial components: the first part computes a segmentation of cell bodies, while the second module identifies the centers of these cells. Our model is trained end-to-end from scratch on a mouse parotid salivary gland stem cell nuclei dataset comprising 107 image stacks from three independent cell preparations, each containing several hundred individual cell nuclei in 3D. In our experiments, we conduct a thorough evaluation of both detection accuracy and segmentation quality, on two different datasets. The results show that the proposed method provides significantly improved detection and segmentation accuracy compared to state-of-the-art and benchmark algorithms. Finally, we use a previously described test-time drop-out strategy to obtain uncertainty estimates on our predictions and validate these estimates by demonstrating that they are strongly correlated with accuracy.

Keywords: Cell nucleus detection, image segmentation, convolutional neural networks, deep learning, confocal microscopy

1 Introduction

Accurate detection and segmentation of individual cell nuclei and sub cellular structures is vital for extracting biological information from microscopy images in order to study complex processes such as morphogenesis [8], gene expression and regulation, disease progression and diagnosis [17]. Despite significant effort, there is a dearth of reliable and robust 3D cell detection and segmentation algorithms, especially in tissues of higher organisms (mice and humans) where these tasks are particularly challenging due to heterogeneous intensity profiles, high variation in cell morphology, low signal-to-noise ratio (SNR), poor depth resolution, and crowding and partial overlapping of cells. A comprehensive review of cell detection and segmentation algorithms can be found in [17].

Kofahi *et al.* [1] propose a cell detection and segmentation algorithm that uses an adaptive multi-scale Laplacian-of-Gaussian (LoG) filtering for detecting cells, and graph-cut optimization to segment each detected cell in 2D. Ram *et al.* [9–11] propose an algorithm where the individual cell nuclei are detected using a fast radial symmetry transform. Each detected cell is then segmented in 3D using a combination of the random walker and watershed algorithms. Nandy *et al.* [8] propose a cell detection and segmentation method for nuclei in 3D tissue images using a robust model-based 2D slice-by-slice image segmentation, followed by a graph-cut optimization to find the 3D cell nuclei. One of the main drawbacks of this approach is the substantial computation time required to detect the cells. Also, they make strong assumptions on the shape of the cells which may vary between applications, thereby limiting generalizability.

Recently, thanks to the increasing availability of large amounts of data and advanced computational resources, machine learning (and especially deep learning) approaches have gained popularity. For example, convolutional neural networks (CNNs) [7] have outperformed the state-of-the-art in many computer vision applications [6]. Similarly, CNNs are successfully applied to medical image analysis problems, including the detection or segmentation of structures in microscopy images [2, 13, 15, 16]. Prior CNN models have been developed for detection (often in 2D) or segmentation in microscopy images. In these applications, detection usually aims to identify the central coordinates (or loci) of certain objects (e.g., cell nuclei), whereas segmentation often refers to the more challenging task of delineating object boundaries. For detection, for example, Xie *et al.* [15, 16] and Sirinukunwattana *et al.* [13] use convolutional networks that generate maps with local maxima that correspond to cell loci. In their influential paper, Ronneberger *et al.* [12] present a CNN architecture called U-Net for general biomedical image segmentation. The U-Net has been applied to a range of segmentation problems, including of cell nuclei.

To our knowledge, cell nuclei detection and cell segmentation have been treated as separate problems in the literature. Yet detection and segmentation, as we define above, are related tasks. For instance, given a segmentation image, detection is usually trivial. Inspired by this co-dependency, in this paper, we propose a 3D convolutional network for jointly segmenting cell nuclei and detecting their centroids in microscopy images. Our model consists of a segmentation convolutional network similar to that of a 3D U-Net that comprises an analysis and a synthesis path, the output of which is then connected to a detection network in order to predict the 3D centers of the cells. This serial architecture is motivated by the observation that the detection task is rather straightforward given a segmentation map, yet annotations are easier to obtain for the detection task.

We train the proposed network using an end-to-end strategy. Our work differs from prior work that used CNNs for cell detection and segmentation in two aspects: 1) we propose a joint 3D convolutional network for cell detection and segmentation in microscopy images, and 2) we empirically validate uncertainty estimates computed via test time dropout [4] and demonstrate its use to improve

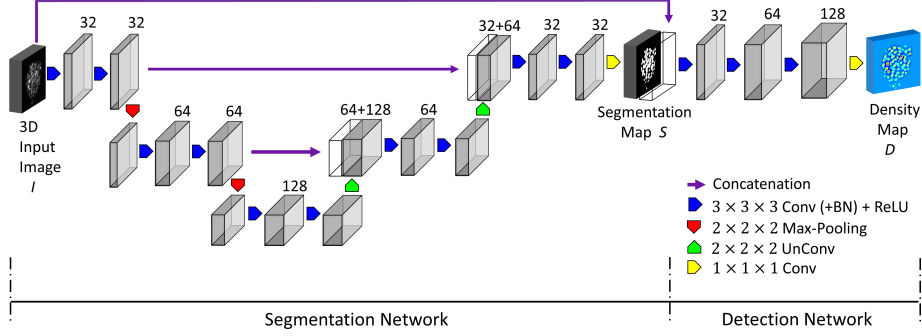


Fig. 1: Proposed 3D convolutional network architecture. Gray boxes represent multi-channel feature maps. White boxes represent the copied feature maps. The number of channels is denoted above each feature map.

final accuracy. We describe our algorithm in detail and present quantitative and qualitative results comparing it to benchmark algorithms.

2 Methods

Let us consider the supervised learning problem of detecting individual 3D cell nuclei. I.e., we are seeking a mapping between a 3D image $I(x)$ and a density volume $D(x) \geq 0$, both defined $\forall x \in \Omega \subset \mathbb{R}^3$. The peaks in the density volume $D(x)$ highlight the locations of cell nuclei, and integrating $D(x)$ over a region gives us the estimated number of cells in that region. We also consider an intermediate representation, $S(x)$, which is a binary segmentation image with the foreground class indicating cell nuclei.

2.1 3D Convolutional Network Architecture

The proposed model consists of two components: a 3D binary segmentation network in the first stage whose output is concatenated along with the original 3D image and fed in as the input to a second module, a 3D detection network that detects cell nuclei centers in the image (see Fig. 1). We define each stage in detail below.

Segmentation Network We adopt the U-Net architecture [2] as the basis of our segmentation network. The motivation behind this architecture is that the contraction and expansion paths of the architecture captures the context around the objects in order to provide a better representation of the object. As in a standard U-Net, we employed three up/down sampling steps and rectified linear units (ReLU) [2] as the activation function. In the contraction path, each layer contains two $3 \times 3 \times 3$ convolutions, and then a $2 \times 2 \times 2$ max pooling (stride of 2 in each dimension). In the expansion path, each layer consists of an up-sampling of $2 \times 2 \times 2$ (UnConv), a concatenation of the cropped feature maps from the corresponding resolution step, and two $3 \times 3 \times 3$ convolutions, with each convolution followed by a ReLU. In the last layer, we use a $1 \times 1 \times 1$ convolution to reduce the number of output channels to a binary segmentation map S

(consisting of either foreground cells or background). In total the segmentation network has 10 convolutional layers.

The input to our segmentation network are $72 \times 72 \times 48$ 3D image patches extracted from the cell nuclei microscopy images. We do not zero-pad the image patches, as we already select patch sizes that are much larger than that of a typical nucleus. The output patches are of size $32 \times 32 \times 8$ and tile the entire 3D volume in a non-overlapping fashion. A graphical representation of the segmentation network architecture is shown in Fig. 1 (see the left side).

Detection Network For cell detection, we propose a 3D convolution regression network that takes in the input 3D image along with the output of the segmentation network and produces a density map $D(x)$ that has high probability values at cell centers. Our detection network has three layers, where each layer consists of a $3 \times 3 \times 3$ convolution followed by a ReLU. In the last layer, we use a $1 \times 1 \times 1$ convolution to reduce the number of output channels to a regressed density map D . The input and output of our detection network are $32 \times 32 \times 8$ image patches. A graphical representation of the detection network architecture is shown in Fig. 1 (see the right side).

2.2 Training

The proposed network is trained in an end-to-end fashion with stochastic gradient descent on a loss function comprising two parts. The first component quantifies segmentation accuracy, and is computed based on the segmentation network output and ground truth segmentations in the training data. The second part of the loss function measures detection accuracy, and is computed based on the ground truth centroid locations of the cell nuclei and the detection network output. In general, the loss function values are evaluated only for available annotations. For example, if for a training data point we only have cell centroids and no segmentations, the segmentation component of the loss function is ignored.

For segmentation, the loss function is the sum of Dice coefficient and weighted cross entropy [12]. The weights for the cross entropy loss are pre-computed for each ground truth segmentation to encourage the separation of cells, as described in [12], but in 3D.

For cell detection, the task is to regress the density volume from the input cell images. To create target ground truth annotations, each 3D centroid location is convolved with a 3D Gaussian filter (with a standard deviation of $1 \mu m$) and superimposed to create the density volume. We use the absolute error (L_1 loss) between the predicted output and the target density volume.

We employed Adam [5] to optimize the weights of the network. We use a mini-batch size of 4. Batch normalization (BN) is introduced before each ReLU in our network during training and the global statistics are updated using these values. The biases are initialized with zero, and the learning rate is initialized to $\alpha = 0.01$ and decreased by a factor of 10 every 10 epochs. The exponential decay rates for the first and second moment estimates are set as $\beta_1 = 0.9$ and $\beta_2 = 0.999$, respectively. We used minimum value of 10^{-8} to prevent division by zero. We also apply a dropout rate of 0.5 as regularization.

We found data augmentation useful for making the network more robust and encode the desired invariance. Each image was randomly rotated between -10 to +10 degrees, and randomly scaled between 0.9 and 1.1 to achieve $5\times$ data augmentation. At test time, given an input image $I(x)$ our trained model predicts the segmentation map $S(x)$ for cell segmentation and the density map $D(x)$ for cell detection. Our code is freely available at *Link Hidden for Anonymity*.

3 Experiments and Results

Dataset 1: We use image stacks of mouse parotid salivary gland stem cells obtained via a laser scanning confocal microscope. The images are of 512×512 in the x- and y-directions and vary between 60 and 110 in the z-direction. We used a total of 107 3D images that contained a total of 42,683 3D cell nuclei. A careful manual detection of 3D cell centroids for all the 107 images and a manual segmentation of the cell nuclei for 23 of the 107 images was performed by an expert and considered for subsequent analysis. The models were trained on 80 3D images (cell centroids were annotated in all, whereas segmentations were manually traced in 15 of these images that contained 5928 cells) and tested on 27 3D images (8 of these had manual segmentations of 3157 cells).

Dataset 2: We also evaluated our trained model on the independent Broad Bioimage Benchmark Collection (BBBC) dataset BBBC024 [3]. This dataset is a synthetic creation of 3D HL60 cell line consisting of 120 3D images with a total of 2400 cell nuclei. Cell centroids and segmentations are available for all images.

3.1 Benchmark Methods

We compared proposed method to a state-of-the-art (SOTA) cell detection method, namely the FRST algorithm [10], and two SOTA cell segmentation methods, the random walker watershed (RWW) algorithm [11], and Stegmaier *et al.*'s method (TWANG) [14]. We also trained two independent models (both based on the 3D U-Net architecture [2]) for cell detection and segmentation, on the same training dataset as the proposed method. These U-Net benchmark models are essentially the “segmentation network” of the proposed architecture (Fig 1) trained only with segmentation or detection loss functions.

3.2 Performance Evaluation

For cell detection, we evaluated all the algorithms using conventional metrics, namely precision $P = TP/(TP + FP)$, recall $R = TP/(TP + FN)$, and the coverage measure $F = 2PR/(P + R)$. Here, TP is the number of true positive detections, FP is the number of false positives, and FN is the number of false negatives. Note that each ground truth nucleus is assigned to at most one predicted nucleus that is present within a $3.28\mu m$ radius. The assigned predicted nucleus is a true positive, and unassigned predicted nuclei are considered false positives. Ground truth nuclei with no assigned predicted nuclei are counted as false negatives. For cell segmentation, we evaluated all the algorithms using the mutual overlap measure (Dice Coefficient), the Hausdorff distance (HD) [11],

Table 1: Performance of the Algorithms For Cell Detection Task

Data	Method	P	R	F
Data set 1	Ours	0.864	0.754	0.805
	FRST	0.621	0.529	0.571
	U-Net	0.796	0.703	0.747
	Ours w/ DO	0.869	0.769	0.816
Data set 2	Ours	0.924	0.901	0.912
	FRST	0.885	0.822	0.852
	U-Net	0.904	0.886	0.895
	Ours w/ DO	0.931	0.919	0.925

Table 2: Performance of the Algorithms For Cell Segmentation Task

Data	Method	Dice	HD	RE
Data set 1	Ours	0.763	8.72	0.0996
	RWW	0.681	10.32	0.1792
	U-Net	0.717	9.63	0.1047
	Ours w/ DO	0.781	8.69	0.0849
Data set 2	Ours	0.934	4.91	0.0287
	RWW	0.892	6.78	0.0663
	U-Net	0.919	5.02	0.0322
	TWANG	—	6.62	0.0618
	Ours w/ DO	0.939	4.82	0.0239

and the Rand error (RE) [12]. The best segmentation algorithm is the one that maximizes the Dice score and minimizes HD and RE.

Table 1 shows quantitative results on the test data of 27 3D images from **Dataset 1**. We observe that the F -score of our proposed 3D convolutional network is 5.8 percentage points greater than the 3D U-Net, and 23.4 percentage points greater than the FRST [10] benchmarks. Fig. 2 shows the qualitative detection results of the compared methods on a sample image from the test data in the **Dataset 1**. Table 2 shows the qualitative results of cell segmentation applied to the test data from **Dataset 1**. We observe that the proposed network achieves the best Dice and lowest RE, and HD values.

We conducted an independent comparison on the synthetic **Dataset 2** (BBBC024). We note that the proposed model was trained on the training data from **Dataset 1**. Quantitative results are presented in Tables 1 and 2. We observe that the proposed network outperforms benchmark methods for both cell detection and cell

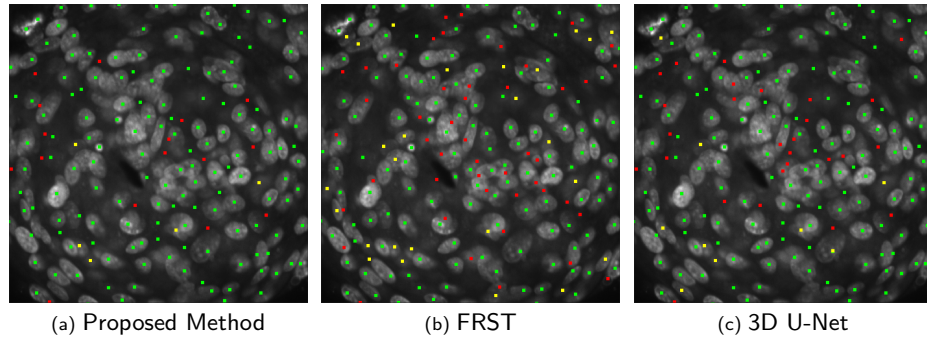


Fig. 2: Cell detection results on a test patch ($512 \times 512 \times 6$) from **Dataset 1**. The TP, FP, and FN, are shown in green, red, and yellow color, respectively.

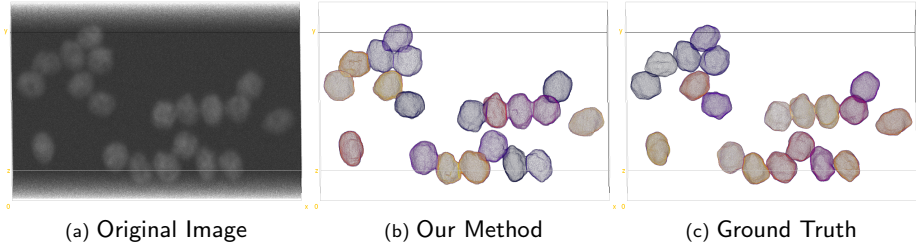


Fig. 3: A 3D rendered view of the segmentation results of our proposed network on a representative image from **Dataset 2**.

segmentation. In Fig. 3, we show qualitative segmentation results of our proposed method on a representative example image from **Dataset 2**.

3.3 Uncertainty Quantification

Accurate estimates of prediction uncertainty can be invaluable in practice, in particular in the downstream use of the predictions. We apply a recently introduced technique for quantifying uncertainty in deep learning models [4], that carries out dropout during test time, which can be viewed as performing Monte Carlo sampling from an approximate posterior distribution.

Here we apply this idea to cell nuclei detection. We perform 100 test time dropouts on **Dataset 1**, obtaining predicted density volumes. The local maxima in these drop-out predictions were considered as candidate cell nuclei. We then computed the distance between the predicted peak (computed without test time drop-out) and the 90th closest drop-out peak to define the radius of the 90th percentile confidence volume. In **Dataset1**, prediction error (distance between the predicted peak and the closest ground truth) was strongly correlated (Pearson’s $r = 0.664$, $P = 0.044$) with the 90% confidence radius, which suggests that the drop-out based-uncertainty estimates correlate well with prediction accuracy. There was a similar correlation in **Dataset2** (Pearson’s $r = 0.723$, $P = 0.029$). Further, removing the predictions with high uncertainty (those with 90th percent confidence radii in the top 10%) leads to an improvement in the detection accuracy (in Table 1, see rows corresponding to “Ours with DO” (Drop-out)).

4 Conclusion

We introduced an end-to-end 3D convolutional network for the problem of joint cell detection and segmentation in microscopy images. We evaluate the proposed model on a synthetic (BBBC024) and real dataset and show that it outperforms SOTA and benchmark methods for both cell detection and the cell segmentation tasks with respect to standard metric. We also, explored the use of quantifying prediction uncertainty via a test-time drop-out strategy and demonstrated that the proposed approach can be used to estimate and improve accuracy.

References

1. Al-Kofahi, Y., Lassoued, W., Lee, W., Roysam, B.: Improved automatic detection and segmentation of cell nuclei in histology images. *IEEE Trans. Biomed. Engg.* 57(4), 841–852 (Apr 2010)
2. Cicek, O., Abdulkadir, A., Lienkamp, S.S., Brox, T., Ronneberger, O.: 3D U-Net: learning dense volumetric segmentation from sparse annotation. In: *Proc. Med. Image Comput. Comput. Assist. Intervention (MICCAI)*. pp. 424–432 (2016)
3. David, S., Michal, K., Stanislav, S.: Generation of digital phantoms of cell nuclei and simulation of image formation in 3D image cytometry. *Cyto. part: A* 75(6), 494–509 (Mar 2009)
4. Gal, Y., Ghahramani, Z.: Dropout as a Bayesian approximation: representing model uncertainty in deep learning. In: *Proc. Intl. Conf. Mach. Learning*. pp. 1050–1059 (2016)
5. Kingma, D., Ba, J.: Adam: a method for stochastic optimization. In: *Proc. 3rd Intl. Conf. Learning Representations* (2015), <https://arxiv.org/pdf/1412.6980.pdf>
6. Krizhevsky, A., Sutskever, I., Hinton, G.: ImageNet classification with deep convolutional neural networks. In: *Proc. Neural Information and Processing Systems*. pp. 1097–1105 (2012)
7. LeCun, Y., Bengio, Y., Hinton, G.: Deep learning. *Nat.* 521(7553), 436–444 (May 2015)
8. Nandy, K., Chellappa, R., Kumar, A., Lockett, S.J.: Segmentation of nuclei from 3D microscopy images of tissue via graphcut optimization. *IEEE Trans. Sel. Topics Signal Process.* 10(1), 140–150 (Feb 2016)
9. Ram, S., Rodríguez, J.J.: Symmetry-based detection of nuclei in microscopy images. In: *Proc. IEEE Intl. Conf. Acoust., Speech, Signal Process.* pp. 1128–1132 (2013)
10. Ram, S., Rodríguez, J.J.: Size-invariant detection of cell nuclei in microscopy images. *IEEE Trans. Med. Imag.* 35(7), 1753–1764 (Jul 2016)
11. Ram, S., Rodríguez, J.J., Bosco, G.: Size-invariant cell nucleus segmentation in 3-D microscopy. In: *Proc. IEEE Southwest Symp. Image Anal. Interp.* pp. 37–40 (2012)
12. Ronneberger, O., Fischer, P., Brox, T.: U-Net: convolutional networks for biomedical image segmentation. In: *Proc. Med. Image Comput. Comput. Assist. Intervention (MICCAI)*. pp. 234–241 (2015)
13. Sirinukunwattana, K., Raza, S.E.A., Tsang, Y.W., Snead, D.R.J., Cree, I.A., Rajpoot, N.M.: Locality sensitive deep learning for detection and classification of nuclei in routine colon cancer histology images. *IEEE Trans. Med. Imag.* 35(5), 1196–1206 (May 2016)
14. Stegmaier, J., Otte, J.C., Kobitski, A., Bartschat, A., Garcia, A., Nienhaus, G.U., Strähle, U., Mikut, R.: Fast segmentation of stained nuclei in terabyte-scale time resolved 3D microscopy image stacks. *PLoS One* 9(2), e90036 (Feb 2014)
15. Xie, W., Noble, J.A., Zisserman, A.: Microscopy cell counting with fully convolutional regression networks. *Comput. Methods Biomech. Biomed. Engg. Imag. Visual.* pp. 1–10 (May 2016)
16. Xie, Y., Xing, F., Shi, X., Su, H., Yang, L.: Efficient and robust cell detection: a structured regression approach. *Med. Imag. Anal.*, In Press (2017)
17. Xing, F., Yang, L.: Robust nucleus/cell detection and segmentation in digital pathology and microscopy images: a comprehensive review. *IEEE Reviews Biomed. Engg.* 9, 234–263 (Jan 2016)